Available online at www.sciencedirect.com

SCIENCE DIRECT®

Engineering Geology 77 (2005) 115–126

ENGINEERING GEOLOGY

www.elsevier.com/locate/enggeo

Treatment for a fully weathered rock dam foundation

Y.S. Wang[a], S.H. Liu[b,*]

[a]*Water Resources and Hydropower Planning and Design General Administration, MWR, Beijing 100011, P.R. China*
[b]*College of Water Conservancy and Hydropower Engineering, Hohai University, Xikang Road 1, Nanjing 210098, PR China*

Received 16 March 2004; accepted 30 August 2004
Available online 12 October 2004

Abstract

The main dam at the upper reservoir of Tianhuanping pumped storage power station is a rockfill dam with an asphalt concrete impervious lining on the upstream face. It is constructed on a non-homogeneous fully weathered rock foundation. In this paper, we present the case study on the treatment for this non-homogeneous fully weathered rock dam foundation. The treatment includes the partial excavation of the fully weathered rock in different depths with respect to the dam deformation, and the enlargement of the transition curvature at the junctions of the inclined dam face and the reservoir floor, as well as the reinforcement for the asphalt concrete impervious lining with a layer of polyester mesh at the parts where tensile strains of the lining are large. A three-dimensional (3D) finite element analysis is carried out for the main dam to provide the basis for the proposed compound treatment method. To account for the effect of the intermediate principal stress σ_2 on the deformation and strength of soils, a simple constitutive soil model is proposed for the finite element (FE) analysis. So far, this project has operated well for more than 5 years without any maintenance for the main dam's asphalt concrete impervious lining, illustrating the success of the treatment for the fully weathered rock dam foundation.

Keywords: Dam; Excavation; Finite element analysis; Full weathering soil; Reinforcement; Treatment

1. Introduction

Tianhuanping pumped storage power station, abbreviated as THP project in this paper, is one of the largest purely pumped storage power stations in China. It was completed in the late 1990s. The total installed capacity of the project is 1800 MW, comprising six units of 300 MW each, with an annual energy output of 3160 GWh. The project consists of an upper and a lower reservoir, a water conveyance system, and an underground powerhouse complex. The horizontal distance between the upper and lower reservoirs is approximately 1 km, with an average water conduit length (L) of 1428 m and an available head (H) of about 570 m. The L/H ratio is only 2.5, among the smallest in the word.

The upper reservoir, located in a natural high depression between Tianhuanping and Getianling mountains, is impounded by one main dam and four saddle (subsidiary) dams with a gross storage capacity

* Corresponding author. Tel.: +81 25 83786727; fax: +86 25 83731332.
E-mail address: sihong_hhu@yahoo.com.cn (S.H. Liu).

0013-7952/$ - see front matter © 2004 Elsevier B.V. All rights reserved.
doi:10.1016/j.enggeo.2004.08.006

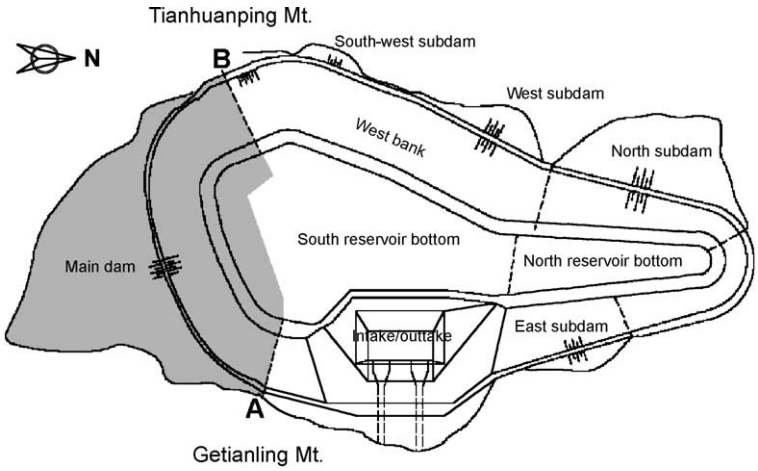

Fig. 1. Upper reservoir of Tianhuangping pumped storage power station.

of 8.85 million m^3 (Fig. 1). The main dam, with a maximum height of 72 m, a crest length of 503 m, a crest width of 8 m, an upstream slope of 1V:2H and an average downstream slope of 1V:2.1H, is an earth-rockfill embankment lined with imperious asphalt concrete at the upstream face and constructed on a full weathering soil foundation of uneven depths. The saddle dams are of similar construction, from 9.3 to 34 m in height. The reservoir basin is lined with asphalt concrete as well to prevent water leakage and to protect the reservoir from erosion during the daily water level fluctuations of up to 42 m.

One of the key and challenging technical problems during the design and construction of the upper reservoir in THP project is the treatment for the fully weathered rock (or termed as "full weathering soil") foundation of uneven depths, especially in the main dam foundation (the shade part in Fig. 1). In this paper, we describe the properties of the full weathering soil and introduce how to treat this full weathering soil in the main dam foundation. The treatment was verified by limiting the tensile strain of the asphalt concrete lining within its allowable value, based on the results of a three-dimensional finite element analysis for the main dam.

2. Distributions and properties of the full weathering soil in the main dam foundation

Numerous cored drill holes and extensive trenches have been made in the area of the upper reservoir of the THP project, which provide a reasonably comprehensive picture of the nature of the underlying bedrock and the depths of weathering (ECIDI, 1990). Fig. 2 shows the geological profile along the main dam axis and Fig. 3 the contour lines of the low limit of the full weathering soil, together with the contour lines of the topography at the site of the main dam. The difference between the low limit of the full

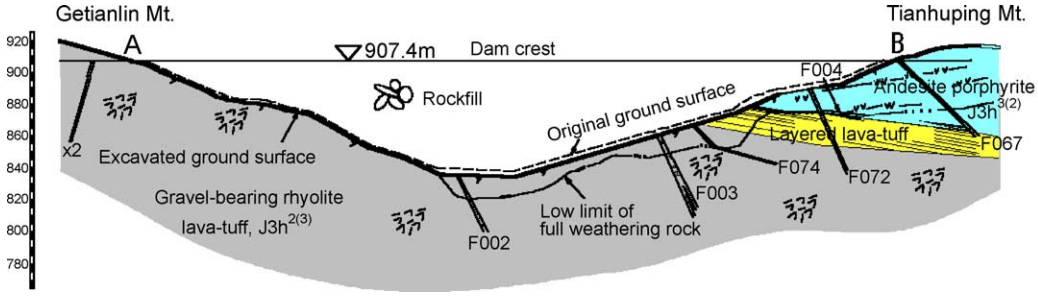

Fig. 2. Geological section along the axis of the main dam.

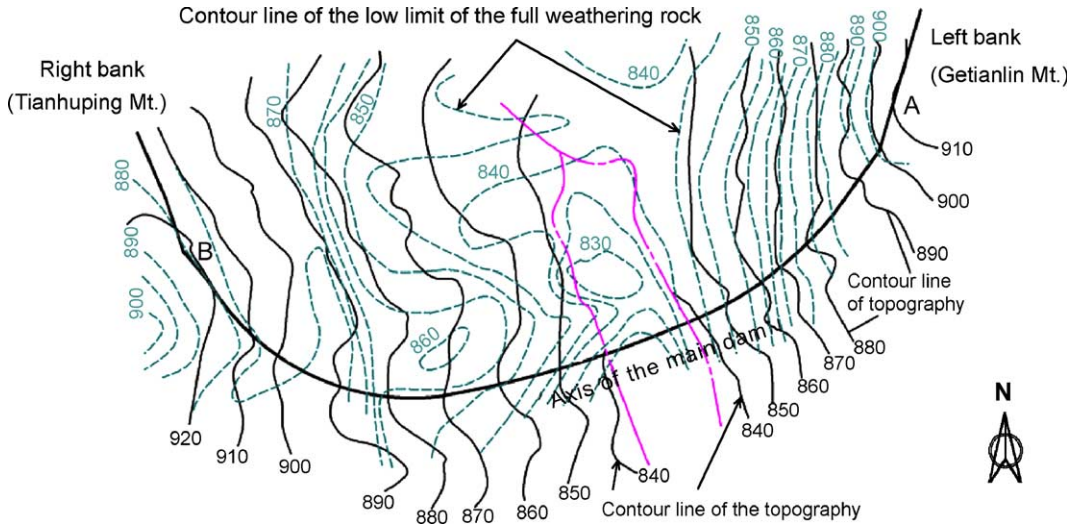

Fig. 3. Contours of the low limit of the full weathering soil (dashed lines) and topography of the main dam (solid lines).

weathering soil and the topography line in Fig. 3 comprises the depth of the full weathering soil. It is known from Fig. 3 that the distribution of the full weathering soil in the main dam foundation has the following characteristics: At the left abutment (roughly the left of the fault F002), the full weathering soil is shallow, commonly with a depth of 3–5 m. In some local places, there are even outcrops of densely or slightly weathered rocks; In the valley bottom, the full weathering soil is commonly 10–17 m thick; however, at the right abutment, about over the elevation of 870 m, the full weathering soil is as thick as 27–35 m where the faults (F003, F004, F067, etc.) are well developed.

The parent rocks of the full weathering soils are mainly gravel-bearing rhyolite lava tuff, andesite porphyrite, and layered rhyolite lava tuff with similar mineral composites of potash feldspar, quartz, kaolinite, and illite. As there is no inclusion of montmorillonite, the full weathering soils are chemi-

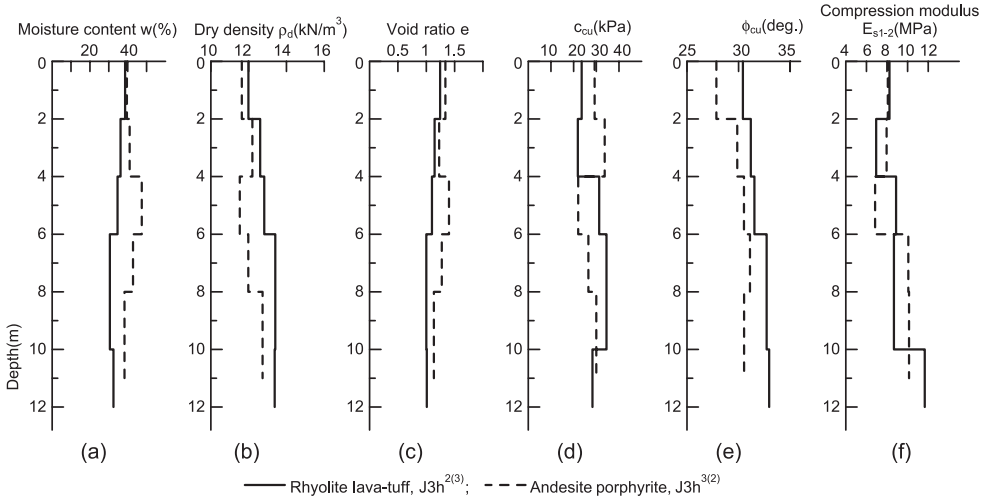

Fig. 4. Properties of the full weathering soil: profiles of (a) moisture content w; (b) dry density; (c) void ratio; (d), (e) cohesion and internal angle of friction obtained from consolidated–undrained triaxial compression tests; (f) compression modulus.

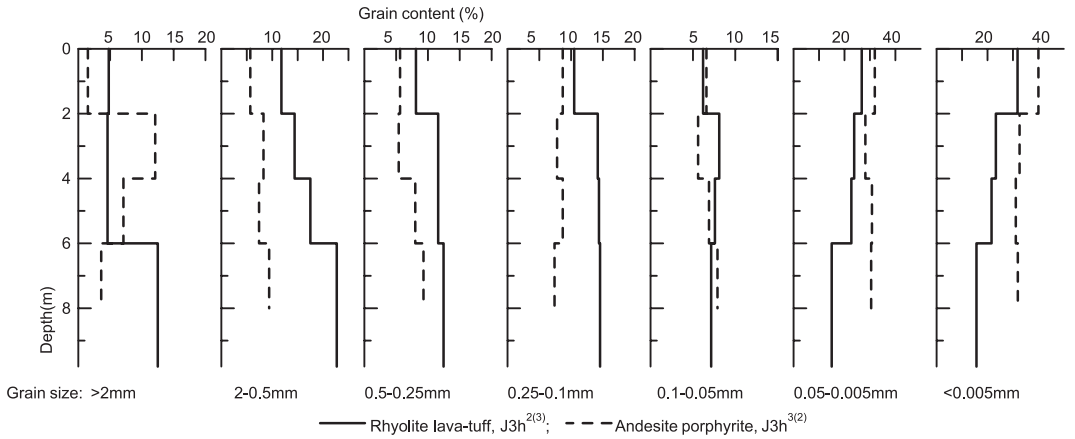

Fig. 5. Profiles of the grain contents of the full weathering soil.

cally inert with a low cation exchange and a weak hydration.

At different stages of the design for the project, a series of laboratory tests have been carried out on about 158 specimens of the full weathering soils sampled mainly within the depth of 10 m. The measured physical and mechanical properties of the full weathering soils are shown in Fig. 4. It can be seen that the full weathering soils of both rhyolite lava-tuff and andesite porphyrite have similar properties. They are common in relatively high moisture content, low dry density and large void ratio, but medium to low compression modulus and relatively high shear strength. For the full weathering soil of rhyolite lava-tuff ($J3h^{2(3)}$), the moisture content and void ratio decrease with the increasing depth, accompanied by an increase in the dry density and shear strength as well as compression modulus, especially when the depth is larger than 4–6 m. For the full weathering soil of andesite porphyrite ($J3h^{3(2)}$), the moisture content and void ratio increase with depth for depths less than 6 m, accompanied by a decrease in compression modulus, but its physical and mechanical behaviors turn to be favorable when the depth is larger than 6 m. Fig. 5 shows the profiles of the grain contents of the full weathering soils. It is seen that for the full weathering soils made of either the rhyolite lava-tuff or the andesite porphyrite, the fine grains (<0.05 mm) decrease while the coarse grains (>0.05 mm) increase with the increasing depth, indicating that the weathering degree decreases with depth. The conclusion that the weathering degree decreases with the increasing depth is also justified by the increase in the measured N-SPT values along the depth, as shown in Fig. 6.

The permeability tests have been performed on four undisturbed samples that were taken in different depths. The results revealed that the seepage failure of the full weathering soils may take place along structural defects. The hydraulic gradients at initial seepage failure and the coefficient of permeability are much greater below a depth of 6 m than at the ground surface (Table 1). Furthermore, the tests on 31 samples taken from trenches or in-situ testing pits

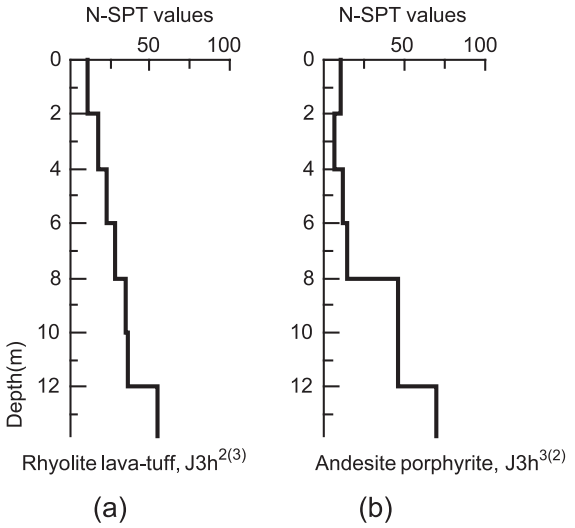

Fig. 6. Profiles of the N-SPT values for the full weathering soil.

Table 1
Average hydraulic gradient and coefficient of permeability of the full weathering soil

Sampling depth (m)	Hydraulic gradient i at initial seepage failure	Coefficient of permeability ($\times 10^{-7}$ m/s)
1–2	0.4–7.9	1.05–7.22
>6	11.0–27.5	2.4–160.0

indicate that less or even no collapse deformation will be induced in the full weathering soils after wetting at the main dam foundation of the THP project.

In the design, such full weathering soil foundation of uneven depths dominated the selection of the lining type of the earth-rockfill dam. Among several alternatives, the asphalt concrete face lining was selected because it suits the uneven deformation of the full weathering soil foundation. However, some engineering measures have to be taken in the full weathering soil foundation of uneven depths; otherwise the large uneven settlement deformation of the foundation will induce large tensile strains in the asphalt concrete lining, causing cracks in the lining.

3. Treatment for the full weathering soil foundation

Four alternatives have been studied for the treatment of the full weathering soil foundation. They are preloading consolidation, dynamic compaction, vibroflotation, and excavation. Due to the high in-situ moisture content in the full weathering soil and the high cost of the construction as well as the limitation of the construction periods, the preloading consolidation method was first rejected. The dynamic compaction and the vibroflotation methods were rejected as well because they may destroy the original skeletons of the full weathering soils and it is difficult to form stone columns in the rock-containing soil foundation. Finally, the excavation method was adopted. However, it is uneconomical and impossible to excavate the entire depth of full weathering soils. By comprehensive analysis of the properties of the full weathering soils, the periods and costs of the construction, we proposed a compound treatment method of the partial excavation of the full weathering soils and the

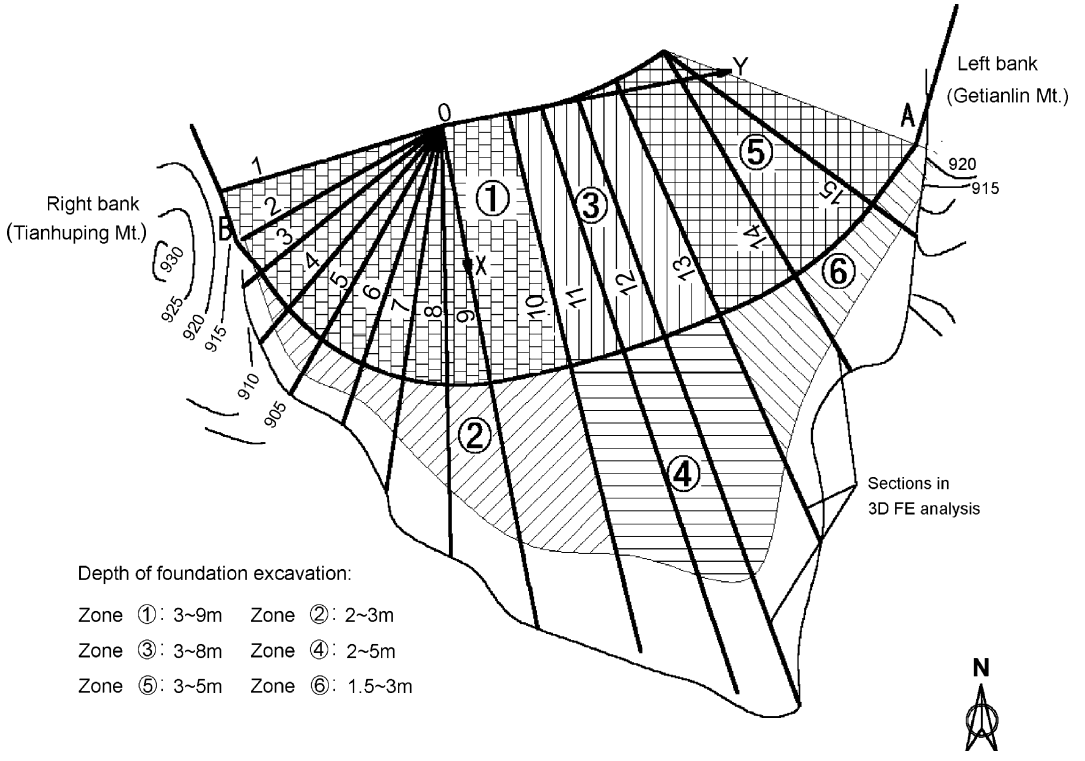

Fig. 7. Depths of excavating the full weathering soil at the foundation of the main dam and the division sections for 3D FE analysis.

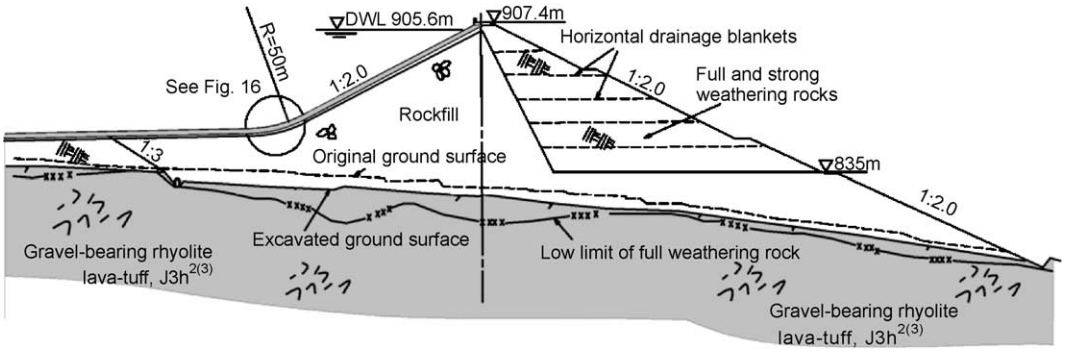

Fig. 8. Cross section 11 of the main dam.

improvement of the asphalt concrete face structure. Fig. 7 shows the excavation depths of the full weathering soils in different zones of the main dam foundation. The excavated surfaces of the full weathering soils were well compacted with a vibrator and then a layer of filter materials with good gradation were placed over them before filling the dam body. The excavation at faults was enlarged somewhat and then backfilled with good filter materials. Some springs exposed in the excavated surfaces were treated with geotextiles combined with filter materials and diverted into the nearest gallery through a drainage trench. The excavated full weathering soils, after mixing with strong weathering rocks, were effectively used to fill the triangular zone at the downstream of the dam above the elevation of 835 m, as shown in Fig. 8. In order to reduce the moisture content of the mixed full and strong weathering rocks, every 5 m lift of the fill is alternated with a 40 cm thick horizontal crushed-stone drainage blanket. The improvement of the asphalt concrete face structure includes the enlargement of the transition curvature at the junctions of the inclined dam face up to 50 m (cf. Fig. 8) and the reservoir floor, as well as the reinforcement for the asphalt concrete impervious lining with a layer of polyester mesh at the parts where the tensile strain of the lining is large.

4. 3D FE analysis to verify the compound treatment

To verify the proposed compound treatment for the full weathering soil dam foundation, a three-dimensional finite element analysis (3D FE analysis), required by the complex geometric shape of the main dam and the uneven depths of the full weathering soil dam foundation, was performed for the main dam.

4.1. Constitutive model of soils applied in the FE analysis

In finite-element analysis, the selection of an appropriate constitutive model primarily involves balancing simplicity with accuracy. Experience has shown that there may be little advantage in using advanced elastoplastic models rather than the simple nonlinear elastic or hyperbolic models for analyzing most earth/rockfill dams, embankments, and stable slopes because the soil mass in those cases is not close to failure. It is considered that nonlinear elastic isotropic stress–strain laws are more properly defined by the tangent bulk modulus K_t and the tangent shear modulus G_t, as the behavior of soil in the separate modes of volume change and shear are reasonably well understood (Naylor, 1978).

The tangent shear modulus G_t is usually determined from conventional triaxial tests (σ_3 = constant) in a similar way as the Duncan and Chang (1970) hyperbolic model. The formulation of the Duncan–Chang hyperbolic stress–strain relationship (cf. Fig. 9(a)) is given by

$$(\sigma_1 - \sigma_3) = \frac{\varepsilon}{\frac{1}{E_i} + \frac{\varepsilon R_f}{(\sigma_1 - \sigma_3)_f}} \quad (1)$$

where σ_1 and σ_3 are the major and minor principal stresses; ε is the axial strain; E_i is the initial Young's

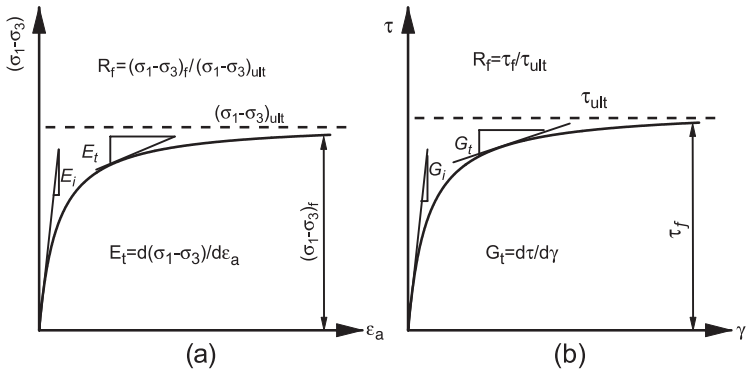

Fig. 9. Hyperbolic stress–strain relations of soils.

modulus; $(\sigma_1-\sigma_3)_f$ is the deviator stress at failure; and the material parameter R_f, referred to as the failure ratio, defines the ratio of the deviator stress at failure to the asymptotic value of deviator stress at large axial strains.

The hyperbolic Eq. (1) can be rewritten so as to be expressed in terms of shear stress τ and strain γ (cf. Fig. 9(b)):

$$\tau = \frac{\gamma}{\frac{1}{G_i} + \frac{\gamma R_f}{\tau_f}} \tag{2}$$

where G_i is the initial tangent shear modulus, and τ_f is the shear stress at failure. The shear stress τ and strain γ are defined as

$$\left.\begin{aligned} \tau &= \frac{\sqrt{2}}{3} q = \frac{1}{3}\sqrt{(\sigma_1-\sigma_2)^2+(\sigma_2-\sigma_3)^2+(\sigma_3-\sigma_1)^2} \\ \gamma &= \sqrt{2}\varepsilon_s = \frac{2}{3}\sqrt{(\varepsilon_1-\varepsilon_2)^2+(\varepsilon_2-\varepsilon_3)^2+(\varepsilon_3-\varepsilon_1)^2} \end{aligned}\right\} \tag{3}$$

From Eqs. (2) and (3), one can obtain the following formulation for the tangent shear modulus G_t according to its definition:

$$G_t = G_i\left(1 - R_f\frac{\tau}{\tau_f}\right)^2 = G_i\left(1 - R_f\frac{q}{q_f}\right)^2 \tag{4}$$

where q is the deviator stress, and q_f is the deviator stress at failure. In most 3D constitutive models of soil, the Extended Mises criterion with a circular shape on the π-plane (the plane in principal stress space at right angles to the line $\sigma_1=\sigma_2=\sigma_3$) is commonly used. Many experimental results show that, compared to the Extended Mises criterion, the Spatially Mobilized Plane (SMP) criterion, which was proposed by Matsuoka and Nakai (1974) and is regarded as a three-dimensional (3D) version of the Mohr–Coulomb criterion, can reflect more realistically the failure of soil in 3D stress state. In particular, it can reflect the larger shear strength at triaxial compression ($\sigma_2=\sigma_3$, Lode's angle $\theta=0^\circ$) than that at triaxial extension ($\sigma_2=\sigma_1$, Lode's angle $\theta=60^\circ$). Moreover, the shape of the SMP criterion on the π-plane develops subsequently from a circle at low stress state to a smoothly convex curve (the solid line in Fig. 10) at high stress state, so that it is better than the Mohr–Coulomb criterion as well in the consistency and continuation of the shear deforma-

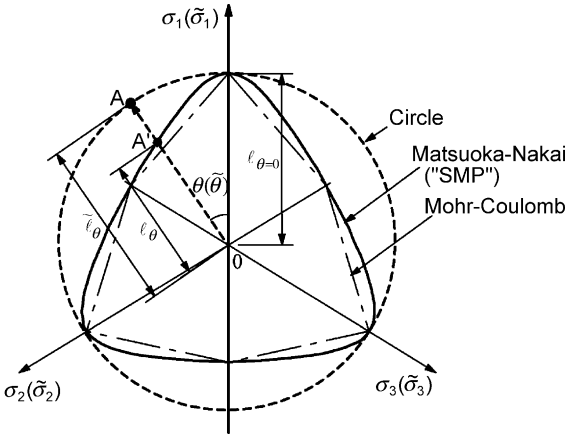

Fig. 10. Shapes of the SMP criterion on π plane before and after the stress is transferred.

tion and the shear failure. The SMP criterion is expressed as

$$\frac{\tau_{\mathrm{SMP}}}{\sigma_{\mathrm{SMP}}}=\sqrt{\frac{I_1I_2-9I_3}{9I_2}}=\text{const.}\quad\text{or}\quad\frac{I_1I_2}{I_3}=\text{const.}\tag{5}$$

where I_1, I_2 and I_3 are the first, second and third effective stress invariants, which are given as follows:

$$\left.\begin{aligned}I_1&=\sigma_1+\sigma_2+\sigma_3\\I_2&=\sigma_1\sigma_2+\sigma_2\sigma_3+\sigma_3\sigma_1\\I_3&=\sigma_1\sigma_2\sigma_3\end{aligned}\right\}\tag{6}$$

In order to adopt the SMP criterion into 3D constitutive models, a transformed stress tensor $\tilde{\sigma}_{ij}$ has been proposed to turn the shape of the SMP criterion on the π-plane from the smoothly convex curve (the solid curve in Fig. 10) to a cone (the broken circle in Fig. 10) in the transformed stress space (Matsuoka et al., 1999). The transformed stress tensor $\tilde{\sigma}_i$ is expressed as

$$\left.\begin{aligned}\tilde{\sigma}_{ij}&=p\delta_{ij}+\tfrac{\ell_0}{\ell_\theta}S_{ij}=p\delta_{ij}+\tfrac{\ell_0}{\sqrt{S_{kl}S_{kl}}}S_{ij}\\\ell_0&=\sqrt{\tfrac{2}{3}}\tfrac{2I_1}{3\sqrt{(I_1I_2-I_3)/(I_1I_2-9I_3)-1}}\end{aligned}\right\}\tag{7}$$

where S_{ij} $(=\sigma_{ij}-p\delta_{ij})$ is the deviator stress tensor; and δ_{ij} is Kronecker's delta.

Adoption of the SMP criterion into the tangent shear modulus G_t requires the deviator stresses in Eq. (4) be expressed in terms of the transformed stresses as defined by Eq. (7), thus Eq. (4) may be rewritten as

$$G_t=G_i\left(1-R_f\frac{\tilde{q}}{\tilde{q}_f}\right)^2\tag{8}$$

As the shape of the SMP criterion on the π-plane is a cone in the transformed stress space (see Fig. 10), the deviator stress at failure $\tilde{q}_f$ is given as follows based on the SMP criterion

$$\tilde{q}_f=M_f\tilde{p}\tag{9}$$

Substituting Eq. (9) into Eq. (8) yields

$$G_t=G_i\left(1-R_f\frac{\tilde{q}}{M_f\tilde{p}}\right)^2\tag{10}$$

where

$$\left.\begin{aligned}\tilde{p}&=\tfrac{1}{3}(\tilde{\sigma}_1+\tilde{\sigma}_2+\tilde{\sigma}_3)=\tfrac{1}{3}\tilde{\sigma}_{ii}\\\tilde{q}&=\tfrac{1}{\sqrt{2}}\sqrt{(\tilde{\sigma}_1-\tilde{\sigma}_2)^2+(\tilde{\sigma}_2-\tilde{\sigma}_3)^2+(\tilde{\sigma}_3-\tilde{\sigma}_1)^2}\\&=\sqrt{\tfrac{3}{2}\left(\tilde{\sigma}_{ij}-\tilde{p}\delta_{ij}\right)\left(\tilde{\sigma}_{ij}-\tilde{p}\delta_{ij}\right)}\\M_f&=\tfrac{6\sin\phi}{3-\sin\phi},\quad\phi\text{ is angle of internal friction}\end{aligned}\right\}\tag{11}$$

The initial tangent shear modulus G_i is computed as follows in a similar way as in the Duncan–Chang model:

$$G_i=kp_a\left(\frac{p}{p_a}\right)^n\tag{12}$$

where k is the tangent shear modulus normalized by p_a when $p=p_a$; n is a non-dimensional modulus exponent; p_a is the atmospheric pressure (100 kPa).

The tangent bulk modulus K_t is determined as

$$K_t=\frac{2(1+v)}{3(1-2v)}G_t\tag{13}$$

where v is Poisson's ratio, typically ranging from 0.3 to 0.4.

4.2. Soil parameters

In the above three-dimensional K–G model, the soil parameters contain k, n, R_f and v as well as the angle of internal friction ϕ. A series of triaxial compression tests have been carried out on 12 specimens of the full weathering soil to determine the soil parameters for the FE analysis, in which four specimens were sampled in cored drill holes and the others were sampled from the testing pits or trenches. As the weathering is different from the sampling locations and the clods of weakly or strongly weathered rock are contained in some specimens, the obtained soil parameters are scattered significantly; for example, the parameter k that characterizes the shear modulus G_t varies from 360 to 23.8. The accurate computation requires the use of different soil parameters corresponding to the sampling locations, but this will make the computation very complicated. In this study, for simplicity, the full weathering soil

Table 2
Soil parameters used in the FE analysis

Material	k	n	R_f	v	ϕ (deg)	γ (kN/m^3)
Full weathering soil	131	0.335	0.58	0.35	30.0	16.0
Rockfill	750	0.68	0.98	0.35	42.5	19.5
Full and strong weathering rocks	300	0.36	0.99	0.35	32.7	19.0
Asphalt concrete lining	310	0.33	0.47	0.35	26.0	24.0

foundation was assumed as a homogeneous medium and the average values of the soil parameters by the tests were used. They are $k = 131$, $n = 0.335$, $R_f = 0.58$ and $\phi = 30^\circ$. The analysis of the test results reveals that the Poisson's ratio v of the full weathering soil varies within the range of 0.3 to 0.4. In the FE analysis, the Poisson's ratio v is thus assumed to be constant with a value of 0.35. By the way, the Electricité de France (EDF, 1991) has provided us the similar average values of $k = 134.5$ and $n = 0.513$ of the full weathering soil, based on their triaxial and unconfined compression tests.

The parameters for other materials involved in the dam structure were either obtained from the tests or determined by our experiences, which are summarized in Table 2.

4.3. FE analysis and results

Fifteen sections perpendicular to the curved dam axis (Fig. 7) separate the main dam body, including the full weathering soil foundation, into 2045 elements with 2483 nodes. The nodes on the low limit of the full weathering soil were treated as vertically constrained. In the analysis, the procedure of the dam construction and the initial reservoir impoundment were simulated in nine steps: five steps for constructing the dam from the bottom to the crest in horizontal layers, one step for constructing the impervious asphalt concrete lining, and three steps for impounding the reservoir up to the design water level of 905.6 m.

As the compression of the full weathering soil foundation is larger than that of the overlying

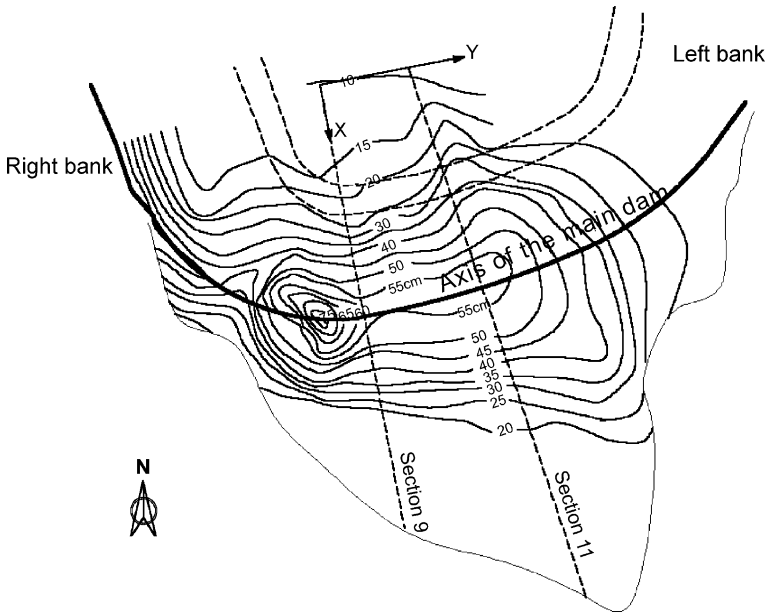

Fig. 11. Contours of the calculated vertical displacements (settlements) at the top surface of the full weathering soil foundation of the main dam at the construction completion.

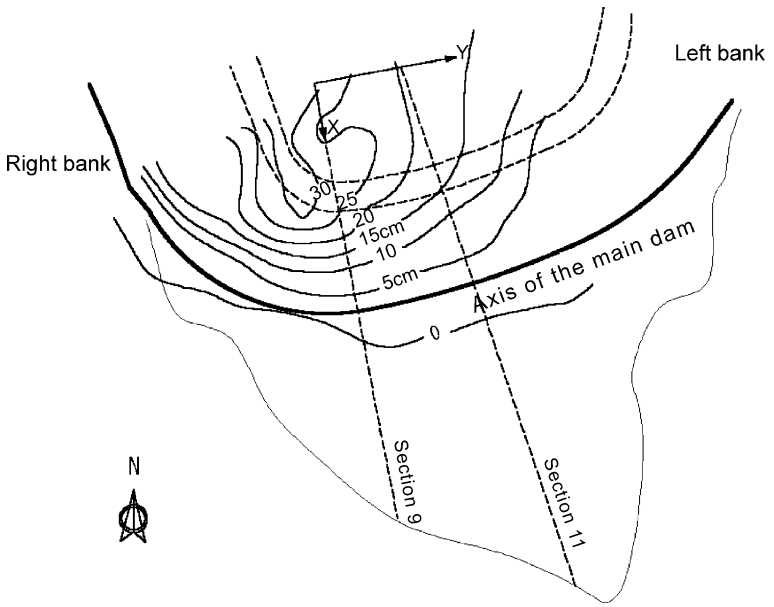

Fig. 12. Contours of the calculated vertical displacements (settlements) at the top surface of the full weathering soil foundation of the main dam due to the first reservoir impoundment.

compacted rockfill, the maximum displacement at the calculated sections takes place typically at the top surface of the full weathering soil foundation. Fig. 11 shows the distribution of the vertical displacements (settlement deformations) on the top surface of the full weathering soil foundation at the completion of the dam construction. The calculated vertical displacement is larger at the right bank than at the left bank, as is the distribution of the depths of the full weathering soil foundation. The maximum value of the calculated vertical displacement at the completion of the dam construction is 75 cm, occurring at the right bank near the dam axis. Fig. 12 shows the distribution of the calculated vertical displacements on the top surface of the full weathering soil foundation due to the reservoir impoundment. It can be seen that the reservoir impoundment causes the vertical displacements mainly in the area with deep full weathering soil foundation on the upstream side of the dam, and there are few increases on the downstream side of the dam. The maximum vertical displacement increase due to the reservoir impoundment is 30 cm, occurring in the curved section at the right bank where the reservoir floor changes sharply and the full weathering soil is deep. The reservoir impoundment also causes downstream-directed horizontal displacements in the upstream area with a maximum value of 17 cm (not shown in figures). Figs. 13 and 14 show the contours of the calculated vertical displacements after the reservoir impoundment at No. 9 and 11 cross sections of the calculation. The maximum vertical displacements of the dam body in Figs. 13 and 14 happen at lower positions due to the high compression of the full weathering soil foundation. No. 11 calculation section, approximately the highest cross section of the main dam, had been well instrumented at different

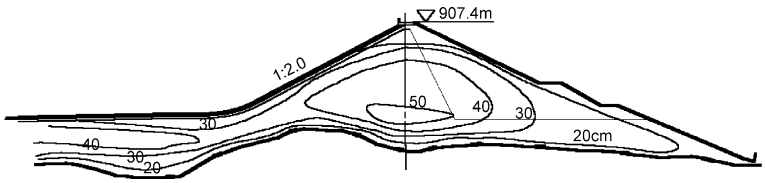

Fig. 13. Contours of the calculated vertical displacements (settlements) at Section 9 after the first reservoir impoundment.

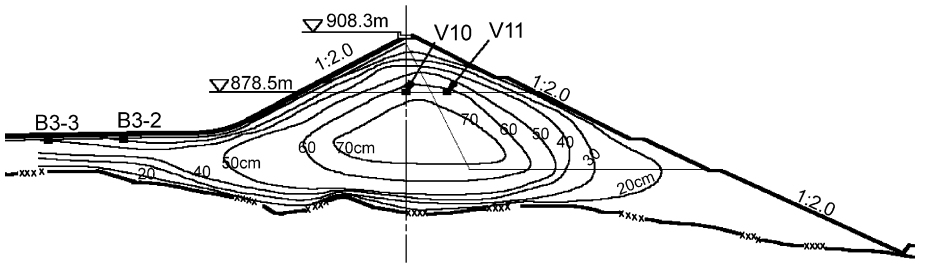

Fig. 14. Contours of the calculated vertical displacements (settlements) at Section 11 after the first reservoir impoundment, together with the locations of four instruments.

elevations to monitor the deformation of the dam; but, unfortunately, most of the equipment was damaged during the construction. Very limited readings on the total vertical settlements have only been taken at the points V10, V11 that were installed inside the dam at the elevation of 878.5 m, and at the points B3-2, B3-3 that were installed near the junctions of the inclined dam face, as illustrated in Fig. 14. Results, measured after the reservoir impoundment, are compared with the calculated values in Table 3. Agreement is reasonable.

Fig. 15 shows the deflections (normal displacements) of the asphalt concrete face lining on some cross sections of the calculation. The maximum deflections occur at the curved part of the asphalt concrete face lining. From the calculation, we found that the tensile strains of the lining are largest at the curved parts as well. The calculated maximum value of the tensile strain of the lining is 0.5%, which is close to the ultimate value of 0.5–1% of the asphalt concrete lining specified in the design. Moreover, the filling materials underlying the curved parts of the asphalt concrete lining are generally difficult to compact in construction. Therefore, we proposed to reinforce the curved part of the asphalt concrete lining with a layer of polyester mesh, as shown in Fig. 16. The polyester mesh used has an allowable tension of 13% and an ultimate tensile strength of 50 kN/m. The polyester mesh reinforcement is modeled in our FE calculation with bar elements that can only withstand tensile forces when they are extended. The calculated maximum tensile strain of the lining is reduced to 1.88×10^{-3} after the reinforcement with the polyester mesh, which is much lower than the ultimate value of 0.5–1% specified in the design.

Table 3
Comparison of the computed and measured vertical settlements after the reservoir impoundment

Instruments	Installed level (m)	Measured value (cm)	Computed value (cm)
V10	∇878.5	64.0	63.5
V11	∇878.5	65.0	62.0
B3-2	∇860.0	23.9	30.0
B3-3	∇860.0	34.1	40.0

5. Conclusions

Owing to the full weathering soil foundation of uneven depths at the dam site, the asphalt concrete faced rockfill dam for the main dam of the upper reservoir in the THP project was selected. Through extensive investigations on the characteristics of the full weathering soil, we proposed a compound treatment for the full weathering soil foundation. It includes the partial excavation of the upper full weathering soil to different depths with respect to

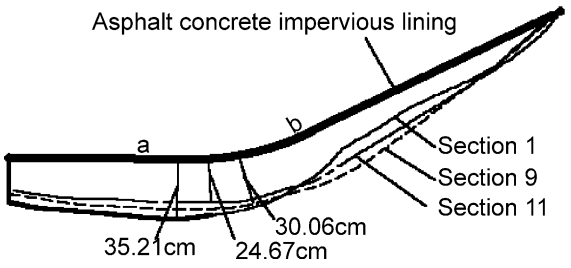

Fig. 15. Deflections (normal displacements) of the asphalt concrete impervious lining due to the first reservoir impoundment at some cross sections of the calculation.

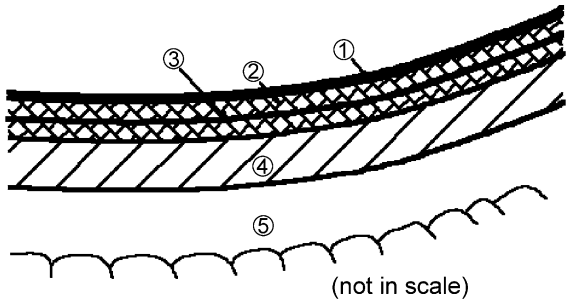

① Protective layer (asphalt mastic)
② Impermeable layer
(fine-grained asphalt concrete)
③ Polyester mesh
④ Levelling layer
(coarse-grained asphalt concrete)
⑤ Transition

Fig. 16. Reinforcement for the asphalt concrete lining at the curved part ("ab" section in Fig. 15) with a layer of polyester mesh that has an allowable tensile strain of 13% and an ultimate tensile strength of 50 kN/m.

the dam deformation, the enlargement of the transition curvature at the junctions of the inclined dam face and the reservoir floor as well as the reinforcement for the asphalt concrete lining at the curved parts with a layer of polyester mesh. The treatment was justified by the three-dimensional finite element analysis for the main dam. The FE analysis indicates that the maximum tensile strain of the asphalt concrete lining is much lower than its allowable value after the treatment. This compound treatment has the advantages of not destroying the original skeletons of the underlying weathering rock (soil), shortening the construction period, and reducing the construction costs. It provides a good engineering example of combining the dam foundation treatment with the selection of the dam type and the modification of the dam shape. The upper reservoir began water filling in July 1998. To date, there have been three full water drawdowns to check the cracks in the asphalt concrete lining. No large cracks have been found in the asphalt concrete face of the main dam where the compound treatment had been implemented, illustrating that the compound treatment for the full weathering soil foundation of the main dam at the upper reservoir of the THP project is successful.

Acknowledgement

The authors wish to acknowledge their former colleagues at East China Investigation and Design Institute for their cooperation in this study.

References

Duncan, J.M., Chang, C.Y., 1970. Nonlinear analysis of stress and strain in soils. ASCE J. Soil Mech. Found. Div. 96, 1629–1653.

East China Investigation and Design Institute (ECIDI), 1990. Geological report of Tianhuangping pumped storage power station project (in Chinese).

Electricité de France (EDF), 1991. Consultative report to the upper reservoir project of Tianhuangping pumped storage power station.

Naylor, D.J., 1978. Stress–strain laws for soils. In: Scott, C.R. (Ed.), Developments in Soil Mechanics. Applied Science Publishers, pp. 39–68.

Matsuoka, H., Nakai, T., 1974. Stress-deformation and strength characteristics of soil under three different principal stresses. Proc JSCE 232, 59–70.

Matsuoka, H., Yao, Y.P., Sun, D.A., 1999. The Cam-clay models revised by the SMP criterion. Soils and Found. 39 (1), 81–95.